Defence Research and Development Canada
Recherche et développement pour la défense Canada

DEFENCE R&D DÉFENSE

Through-Wall Synthetic Aperture Radar (TWSAR) 3D Imaging

Algorithm Design

Greg Barrie

Defence R&D Canada – Ottawa
TECHNICAL MEMORANDUM
DRDC Ottawa TM 2004-224
November 2004

Canada

Through-Wall Synthetic Aperture Radar (TWSAR) 3D Imaging

Algorithm Design

Greg Barrie
Defence R&D Canada – Ottawa

Defence R&D Canada – Ottawa

Technical Memorandum

DRDC Ottawa TM 2004-224

November 2004

Abstract

Typical synthetic aperture radar (SAR) images are two-dimensional, providing range and azimuth information, but furnish few details with respect to elevation. One approach to extend SAR to three-dimensional imaging is to replace the single antenna element by an array of antenna elements. The simplest such implementation of this would be a linear array oriented vertically. This report contains two sections, the first outlining data and image processing for a three-dimensional application, and the second part details *finite beamwidth processing* for the time-domain backprojection method. Standard backprojection implicitly assumes infinite beamwidth, whereby the entire target area is illuminated and returns are collected from all points in the imaging grid. This decreases the efficiency of the algorithm by summing over unnecessary grid points. Finite beamwidth processing is designed to be more physically realistic by accounting for the actual antenna pattern. Initial results show that depending on the width of the effective beam, the number of processing loops can be reduced by up to 50%, while still maintaining good image quality in terms of the reconstructed target response (pulse width). Potential improvements in 3D SAR processing are even greater.

Résumé

Les images typiques de radars à synthèse d'ouverture (SAR) sont bidimensionnelles et fournissent des données de distance et d'azimut, mais peu de détails sur le site. Un moyen d'ajouter une troisième dimension à l'imagerie SAR consiste à remplacer l'élément d'antenne unique par un réseau d'éléments d'antennes. La configuration la plus simple serait un réseau linéaire orienté verticalement. Le rapport se divise en deux parties; la première porte sur le traitement des données et des images dans une application tridimensionnelles, et la seconde examine en détail le traitement de *largeurs de faisceau finies* selon la méthode de rétroprojection dans le domaine temporel. La méthode de rétroprojection courante suppose l'usage d'antennes omnidirectives, au moyen desquelles l'ensemble de la zone cible est illuminé et les échos de tous les points sont recueillis dans la mosaïque radar. Le traitement de largeurs de faisceaux finies est toutefois conçu pour améliorer le réalisme physique en tenant compte du diagramme d'antenne réel. Les résultats initiaux montrent que, selon la largeur du faisceau efficace, on peut réduire le nombre de boucles de traitement de jusqu'à 50 %, tout en maintenant une bonne qualité d'image pour ce qui est de la réponse de cible reconstruite (largeur d'impulsion). Les améliorations possibles pour le traitement RSO 3D sont encore plus importantes.

This page intentionally left blank.

Executive summary

Typical synthetic aperture radar (SAR) images are two-dimensional, providing range and azimuth information, but furnish few details with respect to elevation. In the case of Through-Wall Sensing (TWS) radar, having a third imaging dimension could be easily implemented and be of immediate use in target detection and identification.

This work outlines one approach to extend SAR to three-dimensional imaging: replace the single antenna element by an array of antenna elements. The simplest such implementation is a vertically oriented linear array, and the ensuing transverse motion of the assembly produces data equivalent to that of an extended synthetic *planar* array. Image reconstruction proceeds as before, where range resolution is achieved via pulse compression, azimuth resolution via angular diversity of multiple "look" locations, and the new dimension, elevation, derives from the vertical extent of the physical array. Rather than frequency-domain based reconstruction, the time-domain method of backprojection was selected for this application. It is simple to implement, has localized sidelobes, and it can handle path adjustments for motion compensation and propagation through a dielectric layer such as a building wall.

This report contains two sections, the first outlining data and image processing for a three-dimensional application, and the second part details *finite beamwidth processing* for the time-domain backprojection method. Standard backprojection implicitly assumes omnidirectional antennas, whereby the entire target area is illuminated and returns are collected from all points in the imaging grid. This decreases the efficiency of the algorithm by summing over unnecessary grid points. Finite beamwidth processing, however, is designed to be more physically realistic by accounting for the actual antenna pattern.

This work shows that reducing the effective beamwidth for 2D can reduce the number of processing loops by up to 50%, while still maintaining good image quality in terms of the reconstructed target response (pulse width). Potential improvements in 3D SAR processing are even greater. Simulations carried out in this report indicate there will be an optimum beamwidth: the commonly used omnidirectional configuration provides good results at the cost of excessive iterations while a narrow beamwidth is more efficient, but the image quality is impaired.

Barrie, G. 2004. Through-Wall Synthetic Aperture Radar (TWSAR) 3D Imaging: Algorithm Design. DRDC Ottawa TM 2004-224. Defence R&D Canada – Ottawa.

Sommaire

Les images typiques de radars à synthèse d'ouverture (SAR) sont bidimensionnelles et fournissent des données de distance et d'azimut, mais peu de détails sur le site. Dans le cas du radar de visualisation à travers les murs, une configuration d'imagerie 3D serait facile à mettre en oeuvre et pourrait être utilisée immédiatement pour la détection et l'identification de cibles.

Les présents travaux indiquent comment ajouter une troisième dimension à l'imagerie SAR en remplaçant l'élément d'antenne unique par un réseau d'éléments d'antennes. La configuration la plus simple serait un réseau linéaire orienté verticalement, dont le mouvement transversal produit des données équivalant à celles d'un réseau *plan* synthétique étendu. La reconstruction d'image se fait comme auparavant; la résolution en distance étant obtenue par compression d'impulsions et la résolution en azimut par la diversité angulaire de multiples lieux de visée; la troisième dimension, le site, est obtenue à partir de l'étendue du réseau physique suivant la verticale. Pour cette application, la méthode de rétroprojection dans le domaine temporel a été retenue de préférence à la reconstruction dans le domaine des fréquences. Le réseau est simple à installer et a des lobes latéraux localisés; il permet de régler les trajets de manière à compenser le mouvement et gère la propagation des ondes à travers une couche diélectrique telle qu'un mur de bâtiment.

Le rapport se divise en deux parties; la première porte sur le traitement des données et des images dans une application tridimensionnelles, et la seconde examine en détail le traitement de *largeurs de faisceau finies* selon la méthode de rétroprojection dans le domaine temporel. La méthode de rétroprojection courante suppose l'usage d'antennes omnidirectives, au moyen desquelles l'ensemble de la zone cible est illuminé et les échos de tous les points sont recueillis dans la mosaïque radar. Cette méthode diminue l'efficacité de l'algorithme en faisant la sommation de points inutiles. Le traitement de largeurs de faisceaux finies est toutefois conçu pour améliorer le réalisme physique en tenant compte du diagramme d'antenne réel.

Les présents travaux montrent qu'en diminuant la largeur efficace du faisceau pour le 2D, on peut réduire le nombre de boucles de traitement de jusqu'à 50 %, tout en maintenant une bonne qualité d'image pour ce qui est de la réponse de cible reconstruite (largeur d'impulsion). Les améliorations possibles pour le traitement SAR 3D sont encore plus importantes. Les simulations effectuées dans le cadre des travaux prévoient une largeur de faisceau optimale : la configuration omnidirective couramment utilisée produit de bons résultats au prix d'itérations excessives, alors qu'une faible largeur de faisceau s'avère plus efficace, la qualité de l'image étant toutefois dégradée.

Barrie, G. 2004. Through-Wall Synthetic Aperture Radar (TWSAR) 3D Imaging: Algorithm Design. DRDC Ottawa TM 2004-224. R & D pour la défense Canada – Ottawa.

Table of contents

List of figures

List of tables

This page intentionally left blank.

1. Introduction

Typical SAR images are two-dimensional, providing range and azimuth information, but furnish little detail with respect to elevation. The underlying principle is that transverse motion of a single (point) antenna element generates, or *synthesizes*, a data set equivalent to that produced by an extended linear array.

In three-dimensional imaging, we can readily extend the concepts from two-dimensional SAR by increasing the dimensionality of the generating element by one. That is, the single zero-dimensional element is replaced with a one-dimensional linear array. It follows that transverse motion of this array, oriented perpendicular to the direction of motion, produces data approximating an extended two-dimensional *planar* array. The ensuing reconstruction proceeds as before where range resolution is achieved via pulse compression, azimuth resolution via angular diversity of multiple "look" locations, and the new dimension, elevation, derives from the vertical extent of the physical array.

This report contains two sections, the first outlining data and image processing for a three-dimensional application, and the second part details *finite beamwidth processing* for the time-domain backprojection method. Standard backprojection implicitly assumes omnidirectional antennas, whereby the entire target area is illuminated and returns are collected from all points in the imaging grid. This decreases the efficiency of the algorithm by summing over unnecessary grid points. Finite beamwidth processing is designed to be more physically realistic by accounting for the actual antenna pattern.

Within the context of radar imaging, we can consider three different coordinate systems, defined as the object, data and image space, portrayed in Figure 1.

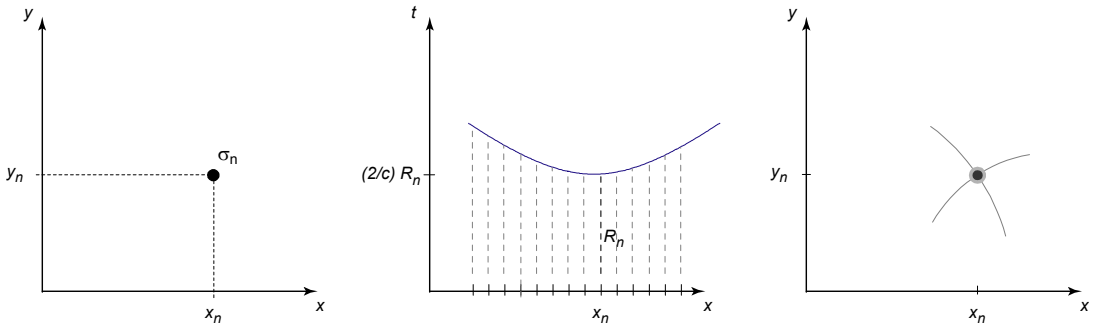

a). object space: g(x,y) *b).* data space: d(x,t) *c).* image space: f(x,y)

Figure 1. *Coordinate systems used in synthetic aperture imaging. (Images are for 2D; extension to 3D is described in text.)*

The object space $g(x,y,z)$, is the actual physical volume (spatial domain) illuminated by the radar. The results of SAR data acquisition and pulse compression are captured

in the data space, $d(x,z,t)$. The range value *R* and return time delay *t* are interchangeable via the transformation $t = 2R/c$. In moving from 2D to 3D, the components that make up *R* are modified to include elevation-dependent range, for example, $R_{2D} = \sqrt{x^2 + y^2}$ vs. $R_{3D} = \sqrt{x^2 + y^2 + z^2}$.

In data space, the echoes for a given point target trace out a hyperbola due to the motion of the radar. The two-dimensional function representing this "spreading" of signal energy is called the *point spread response* (PSR). Energy contained within the PSR must be collected, or focused back to the original point function, within the domain of image space, $f(x,y,z)$.

The extension from two to three dimensions is straightforward:

2D	**3D**
$g(x,y)$	$g(x,y,z)$
$d(x,t)$	$d(x,z,t)$
$f(x,y)$	$f(x,y,z)$

2. Three-dimensional SAR

2.1 System geometry

Here *x* denotes cross-range, or *azimuth*, *y*, the range coordinate and *z* is elevation (refer to Figure 2). By collecting and processing radar data, one attempts to reconstruct an image of objects contained within this area. For a simple system model, we consider a discrete set of point-reflectors with reflectivity σ_p, $(p = 1,2,\cdots)$, at coordinates (x_p, y_p, z_p).

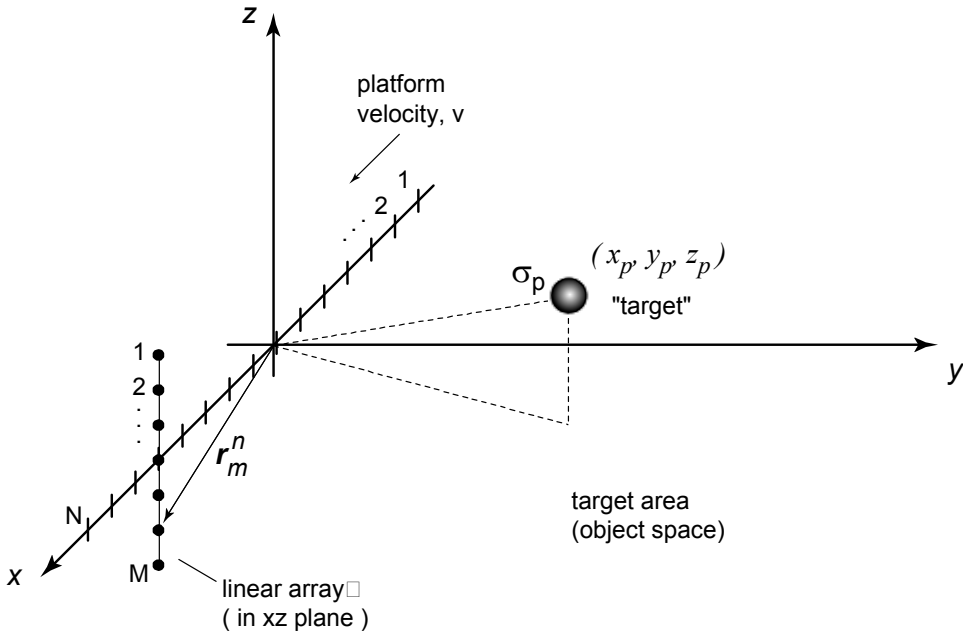

Figure 2. *3D imaging geometry.*

2.2 Array components

The linear array contains *M* elements, each located at position vector $\vec{r}_m$ where $\vec{r}_m = (u_m, v_m, w_m)$, $m = 1,2\ldots,M$. The *u*,*v* and *w* are cartesian coordinates. Further, there are a number of synthetic array positions $n = 1,2\ldots,N$ over which the linear array traverses, resulting in *M* **x** *N* antenna element coordinates[1].

[1] It is difficult to find a clear and consistent way to develop the notation required for this discussion, but Soumekh's text [1] provided a good starting point.

For example, an $M = 5$ element linear array moving across $N = 100$ synthetic array positions would generate in the processor memory a *5 x 100* element matrix. Consequently, the position vector of the m[th] array element at the n[th] synthetic aperture position is $\vec{r}_m^{\,n} = \left(u_m^n, v_m^n, w_m^n\right)$.

2.3 SAR processor

Backprojection is a correlation implementation of matched-filtering. A detailed description of the backprojection method, along with implementation details can be found in [2]. Presently, it suffices that the idea is to correlate data collected at each aperture position as a function of round-trip delay time. This means the correlation is performed with respect to the point spread response (PSR) obtained in the space-time data domain.

Backprojection sums the sampled radar returns for each array element (pixel) of the image map. The signal obtained at each aperture position is time-shifted to match, or align, with a particular pixel element in the image map. Following this, responses across all aperture positions are combined in the image space.

2.4 Channel data

For 3D imaging, the target echo reaching the receiver will be delayed due to the time of propagation between the Tx/Rx array and the target. As specified earlier, "targets" characterized by reflectivity σ_p are located at positions $\left(x_p, y_p, z_p\right)$, while the array element is located at $\left(u, v, w\right)$. Application of this yields the following signal from scattering point 1:

$$s_1\left(\vec{r}\,;t\right) = \sigma_1 \; A\left(t - \frac{2}{c}\sqrt{\left(x_1 - u\right)^2 + \left(y_1 - v\right)^2 + \left(z_1 - w\right)^2} \right), \qquad (1)$$

which is a function of antenna element position, and implicitly is a function of time, t as a consequence of propagation delay. In this expression, $A\left(t - \tau\right)$ is the impulse response of the equipment in the transmit path, including additional system impairments.

The composite signal received at a given array element is the summation of responses from all scattering points (see Figure 3) —

$$\begin{aligned} s\left(\vec{r}\,;t\right) &= \sum_p \sigma_p \; A\left(t - \frac{2}{c}\sqrt{\left(x_p - u\right)^2 + \left(y_p - v\right)^2 + \left(z_p - w\right)^2} \right). \\ &= s_1\left(\vec{r}\,;t\right) + s_2\left(\vec{r}\,;t\right) + \ldots \end{aligned} \qquad (2)$$

Note: To keep the discussion simple, expressions derived here are for the monostatic

case. To consider bistatic configurations as depicted in the diagrams, replace *2R/c* by $(R_{Tx} + R_{Rx})/c$. The bistatic case was implemented in computer code.

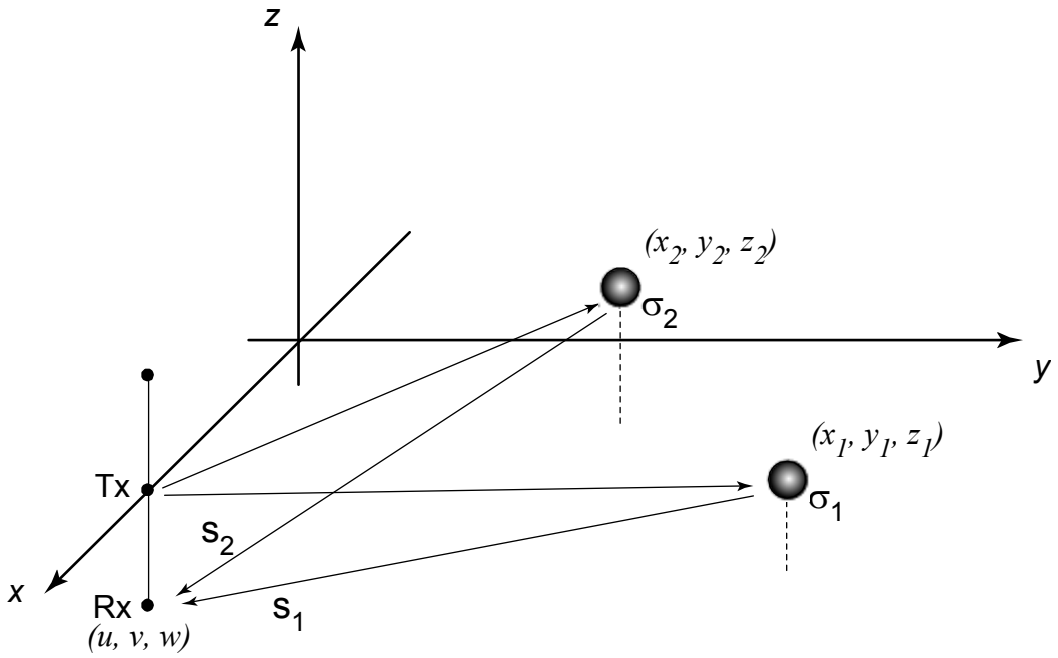

Figure 3. *Composite signal received at array elements.*

As the radar array traverses the synthetic aperture, signals containing combined echoes from all targets are received at each aperture position. The collection of data over all element positions defines the data space. An example of simulated channel data is shown in Figure 4. The column on the left-hand side shows the echos received at various points along the linear array. Each antenna is referred to as a channel, and there are nine elements in this particular array. The received data from odd numbered channels is shown. The column on the right-hand side shows data that has been collected together from multiple aperture positions. The one-dimensional data set corresponding to frame number 41 is indicated by the arrow. Combining multiple frames results in the two-dimensional azimuth vs. range delay images as shown.

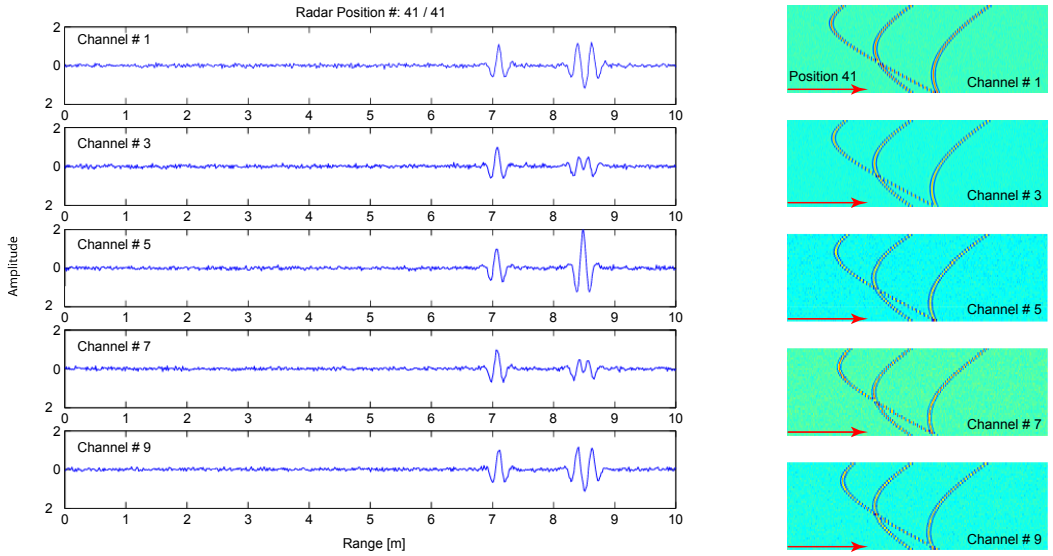

Figure 4. *Channel data for scattering centers at (2,2,0), (5,5,2) and (8,8,4). Units are in meters.*

2.5 Image formation

Energy contained within the curves must be collected, or *focused* back to the original point function. The "optimum" focusing of synthetic aperture data is obtained by correlating collected data $s(\vec{r};t)$ with the SAR signature at a given grid point, (x_i, y_j, z_k). In effect, we require a space-time domain matched filter with respect to $\delta(\vec{r};t)$, yielding a measure of the reflectivity at that point:

$$f(x_i, y_j, z_k) = \int_{\vec{r}} \int_{t} s(\vec{r};t)\; A\left[t - \frac{2}{c}\sqrt{(x_i - u)^2 + (y_j - v)^2 + (z_k - w)^2} \right] dt\; d\vec{r}. \quad (3)$$

where $\vec{r}$ is the position vector of the antenna receive elements as shown in Figure 2 on page 3. Approximating the SAR signature as a delta function, $A(\cdot) \rightarrow \delta(\cdot)$, we obtain

$$\begin{aligned} f(x_i, y_j, z_k) &= \int_{\vec{r}} s\left(\vec{r}; \frac{2}{c}\sqrt{(x_i - u)^2 + (y_j - v)^2 + (z_k - w)^2} \right) d\vec{r} \\ &= \int_{\vec{r}} s\left(\vec{r}; t_{ijk}(\vec{r})\right) d\vec{r} \end{aligned} \quad (4)$$

The time convolution is calculated as —

$$
\begin{aligned}
s\left(\vec{r};t_{ijk}\left(\vec{r}\right)\right) &= s\left(\vec{r};t\right)*\delta\left(-t\right) \\
&= \int_t s\left(\vec{r};t\right)\delta\left(t-\frac{2}{c}\sqrt{\left(x_i-u\right)^2+\left(y_j-v\right)^2+\left(z_k-w\right)^2}\right)dt \\
&= s\left(\vec{r};\ \frac{2}{c}\sqrt{\left(x_i-u\right)^2+\left(y_j-v\right)^2+\left(z_k-w\right)^2}\right)
\end{aligned}
\qquad (5)
$$

Returning to the reflectivity function, the full image is obtained by calculating $f\left(x_i, y_j, z_k\right)$ for each grid point in the image space. In practice, the correlation integral is not computed directly. Due to the incremental nature of both aperture positions and time samples, a two-dimensional discrete summation is performed. Further, a portion of the calculation requires interpolation since the recorded time samples do not correspond exactly to grid locations.

Figure 5 is a representation of discrete targets producing point spread responses (PSR's) in the space-time domain. This diagram shows why the resolution in elevation is so limited. In comparison with horizontal displacement, there are only a limited number of elements along the vertical array, and a correspondingly reduced number of points to focus. An extended, albeit unrealistic, array 10m in length would yield a PSR surface as in Figure 6.

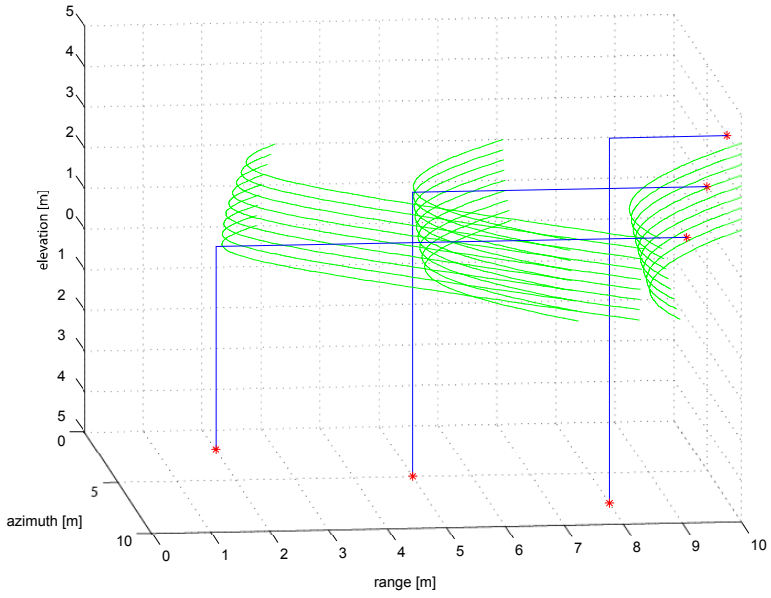

Figure 5. *PSR's for scattering centers at (2,2,0), (5,5,2) and (8,8,4). Units are in meters. Simulated antenna length is 2m, with element spacing equal to 0.25m.*

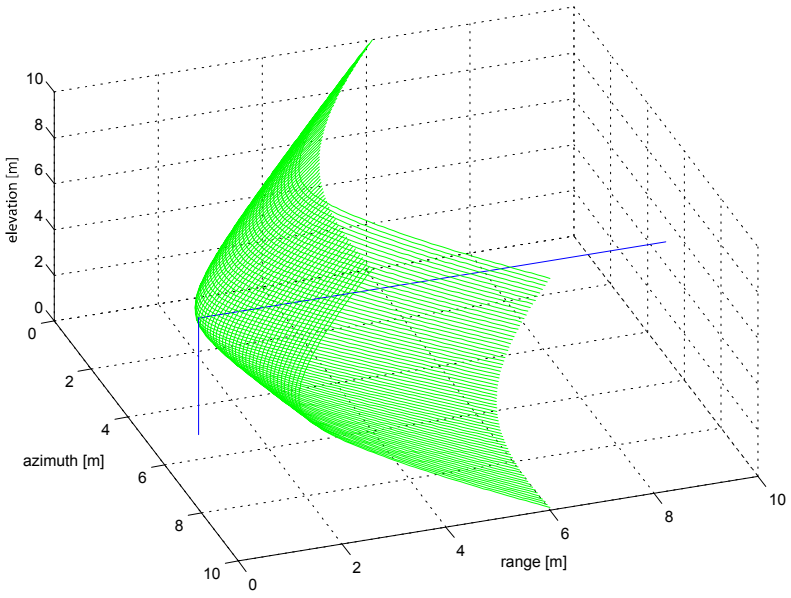

Figure 6. *PSR surface for extended vertical array.*

There are *N* positions in the synthetic aperture, and *M* positions (channels) in the physical array. Grid points are denoted (x_i, y_j, z_k). Therefore, in the discrete computation, we will have a total of five nested loops to perform the required summations *(I x J x K) x N x M*.

2.6 Positioning errors

In an ideal case, the antenna array is constrained to the *x-z* plane and therefore has no *y* (range) component (that is, *v = 0*). In general, the trajectory followed by the system will not be as precise nor will it be as predictable. There will always be some error in the presumed positioning of the Tx/Rx array, and this will influence the precision with which images can be reconstructed. An operational system will have methods put in place to track and compensate for these deviations.

In terms of modeling the effects of positioning errors, these could be accounted for by writing the generalized position vector:

$$\vec{r}_{\delta} = \vec{r} + \vec{\delta} = (u + \delta u, v + \delta v, w + \delta w), \qquad (6)$$

and defining random position errors. This approach to predicting system performance has been carried out for the two-dimensional case [3], but can be generalized to the three-dimensional case by recognizing there are five degrees of freedom to the array's spatial orientation: the position vector for the center of mass and the orientation angles for azimuth and elevation (Figure 7):

$$(x_i, y_i, z_i) \qquad \vec{r} \in V$$

$$\varphi_i \qquad 0 \le \varphi_i < 2\pi$$

$$\theta_i \qquad 0 \le \theta_i \le \pi$$

where V is the imaging volume. This is sufficient to characterize the array since each of the elements are constrained to lie along a line with fixed element spacing. For the remainder of this report however, we assume the element positions are known accurately.

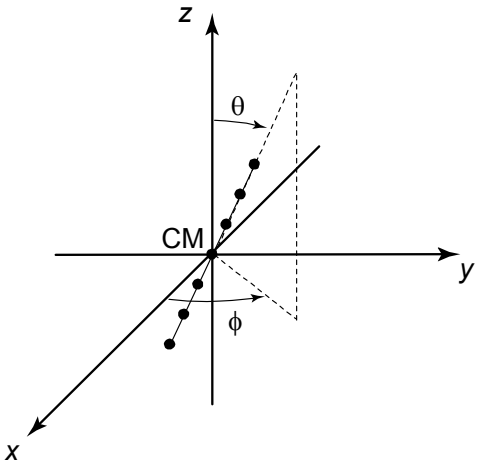

Figure 7. *Random orientation of linear array. Center of mass (CM) corresponds to origin.*

3. Backprojection techniques

3.1 Standard backprojection

A major concern in synthetic aperture imaging application of backprojection techniques involves the high computational effort. For each element of the synthetic aperture, one is forced to consider the contribution from each grid point within the imaging area or volume.

To perform the required processing, the algorithm requires position information for both Tx and Rx elements as well as all of the imaging grid points (refer to Figure 8). This allows calculation of forward and reverse paths, resulting in a value for the 2-way path, which is ultimately rescaled in terms of the time delay.

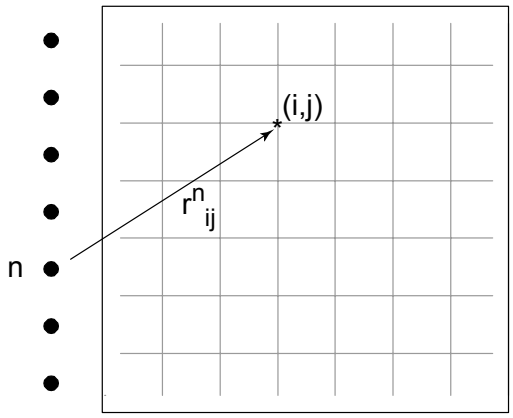

Figure 8. *Geometry for range calculation based on n^{th} array element and grid point (i,j).*

The backprojection algorithm then matches this calculated delay against recorded data, either voltage or field strength vs. time, interpolating the amplitude, $\hat{A}_{ij}^{n}$ received at that grid point (Figure 9). This is generally an interpolated value because delay times rarely correspond to precise sampling points.

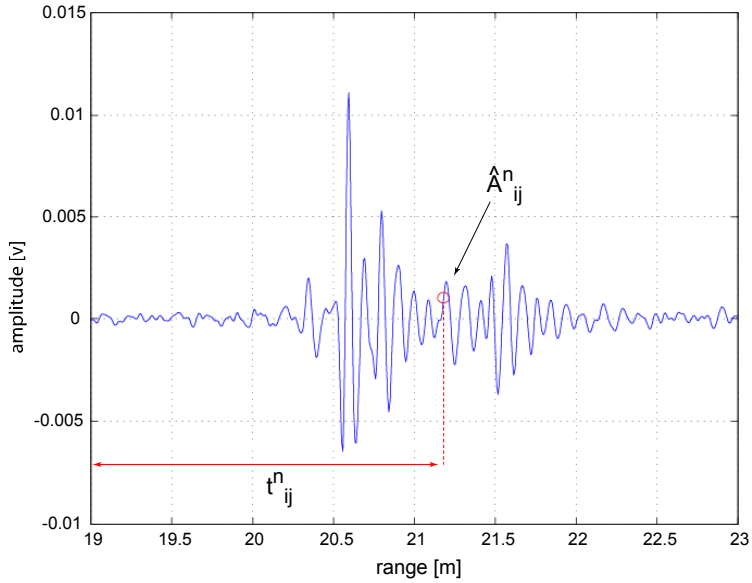

Figure 9. *Amplitude interpolation based on time delay for sensor position n and grid coordinates (i,j).*

To clarify notation, the " ^ " indicates this is an estimated data value obtained from the n[th] channel (aperture position), and is allocated to the grid position *(i,j)*.

A straightforward generalization of this for 3D imaging is $\hat{A}_{ijk}^{nm}$. In this case, *n* remains the synthetic array position while *m* denotes the physical array element position along the vertically oriented linear array. Grid positions for the three-dimensional image space are labelled *(i,j,k)*.

The problem with this technique is that a certain amount of energy is spread, or dispersed, throughout the imaging grid, attributed to points from which it did not originate. As a consequence, one particular field value is applied to a number of points, as indicated in Figure 10. Consider a situation where the time increment is $\pm\Delta_t$. The value $\hat{A}_{ij}^{n}$ is then applied to all grid points falling within the range $r_{ij}^{n} \pm \Delta_r$, creating artifacts along this band. This non-uniqueness is a characteristic of inverse problems where a distinct input does not result in a distinct output–there exist a range of values that satisfy the initial conditions.

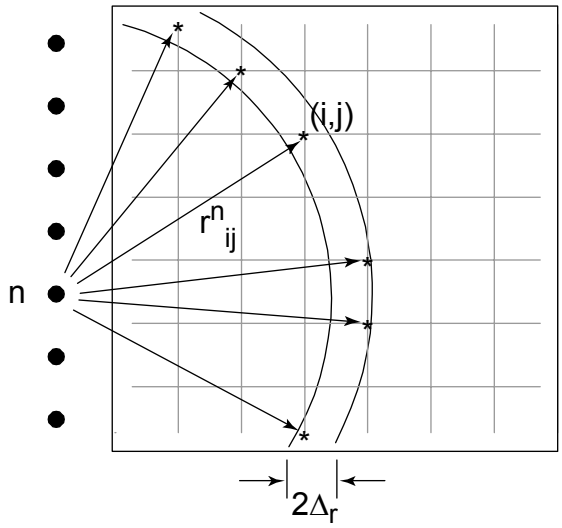

Figure 10. *Schematic of image grid assignment based on interpolated data (omnidirectional antenna).*

This is mitigated somewhat by the principle of constructive interference — the grid points corresponding to persistent targets will continually get reinforced with each aperture position, increasing the SNR, while other influences fade into the background noise.

3.2 Finite beamwidth processing for 2D

Implicit in this approach is the assumption that the antennas are isotropic. In a strip map application such as this, the integration angle approaches 180^o, and in the limit, approaches an infinite aperture. This is certainly the easiest implementation since loops over grid coordinates are unrestricted. A more realistic situation is portrayed in Figure 11, where the antenna possesses a finite beamwidth, Θ.

In this situation, the shaded area represents the area of illumination, where the beamwidth is set arbitrarily at say, the 3 or 10 dB points. The purpose of this is that points outside of the shaded area are neither illuminated, nor do they produce a radar return. There is still some degree of non-uniqueness, but the reduced beamwidth reduces its extent.

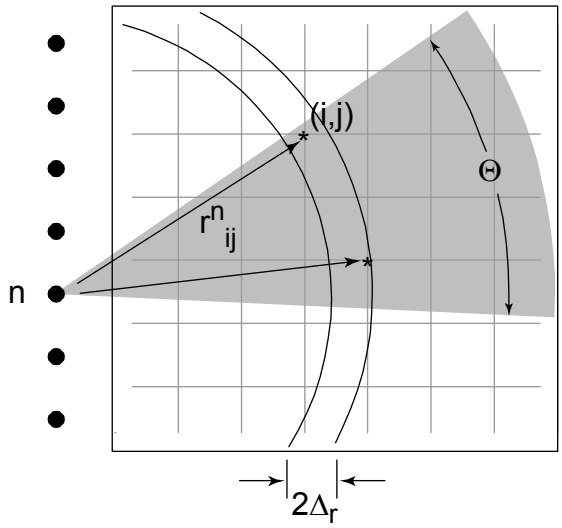

Figure 11. *Finite beamwidth grid point assignment.*

To implement this, we require a method to limit the grid points to those that lie within the illumination area. For the particular case considered here, namely a strip-map SAR routine, the beam axis is always oriented perpendicular to the path of motion. The more general case as depicted in Figure 11 is more appropriate for squint or spotlight-SAR applications, which are not considered in this report. To work through the details of the algorithm, refer to Figure 12.

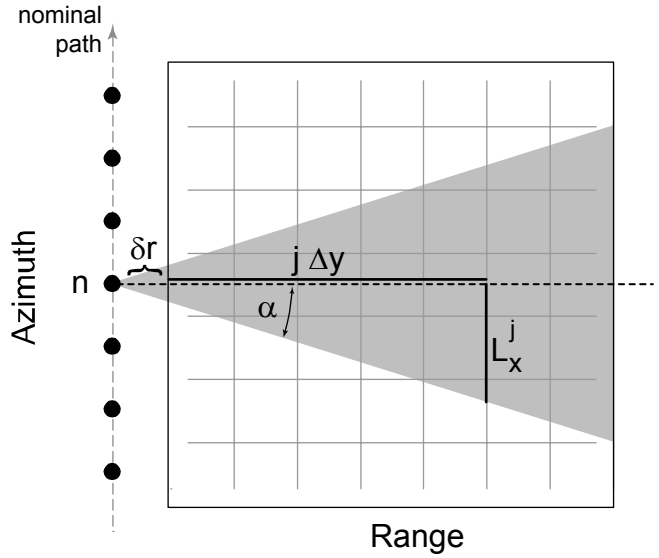

Figure 12. *Parameters used in finite beamwidth processing.*

First, note the grid spacing for azimuth and range respectively, $\Delta x, \Delta y$ which are used as the basic units of distance in the following text. Next, the nth synthetic aperture element is located at $\left(x^n, y^n\right)$. The trajectory of the radar platform can be displaced

from the nominal path, and this is referred to as the "offset." Offset is denoted simply as $\delta r = y^n$, and this value will be positive or negative depending on its position relative to the nominal path. By definition, the range of the imaging grid extends from $y = 0$ to y_{max}. The offset is therefore used to account for path deviation off of the *y*-axis. The outer loop is for range values, moving from $y = 0$ out to the maximum range. At each synthetic aperture (SA) position, we look downrange to grid element *j* (that is, along the perpendicular). The total range from SA element to grid point *j* is therefore $\delta r + j\Delta y$ (refer to Figure 12).

We have specified the antenna half-beamwidth as $\alpha = \Theta / 2$, and can now calculate the azimuth extent for a given range, L_x^j:

$$L_x^j = \left(\delta r + j\Delta y\right)\tan\alpha \qquad (7)$$

This value now has to be converted into upper and lower index values for the grid points. To place L_x^j in its proper location in the imaging grid, we need the x-component of the nth aperture position, x^n. To obtain the lower (or left-hand) limit, subtract the azimuth segment from x^n and divide by the grid spacing, Δx. To stay within the illuminated area, take the upper integer bound. For the upper (or right-hand) limit, we add the segment to x^n and take the lower integer bound. The loop across *x* grid coordinates at a given range increment *j*, for synthetic aperture *n* is therefore:

$$\left\lceil \frac{x^n - L_x^j}{\Delta x} \right\rceil \quad : \quad i \quad : \quad \left\lfloor \frac{x^n + L_x^j}{\Delta x} \right\rfloor. \qquad (8)$$

Contrast this to the routine without modification. In that situation, the loop runs from $1 \le i \le DX$.

The following graphs depict a progression of imaging grids corresponding to different locations for the radar platform (Figure 13). From top to bottom of each column, the radar moves from the upper to lower left-hand corner. There are five aperture positions in total, which is artificially low, but still serves to compare focusing of targets–there are two in the image, somewhere along each arc. At this time in the reconstruction process, the azimuth remains undetermined. Moving from left to right, the effective beamwidth, and therefore the illumination area, is reduced from that of an omnidirectional (~360^o) antenna to approximately 45^o.

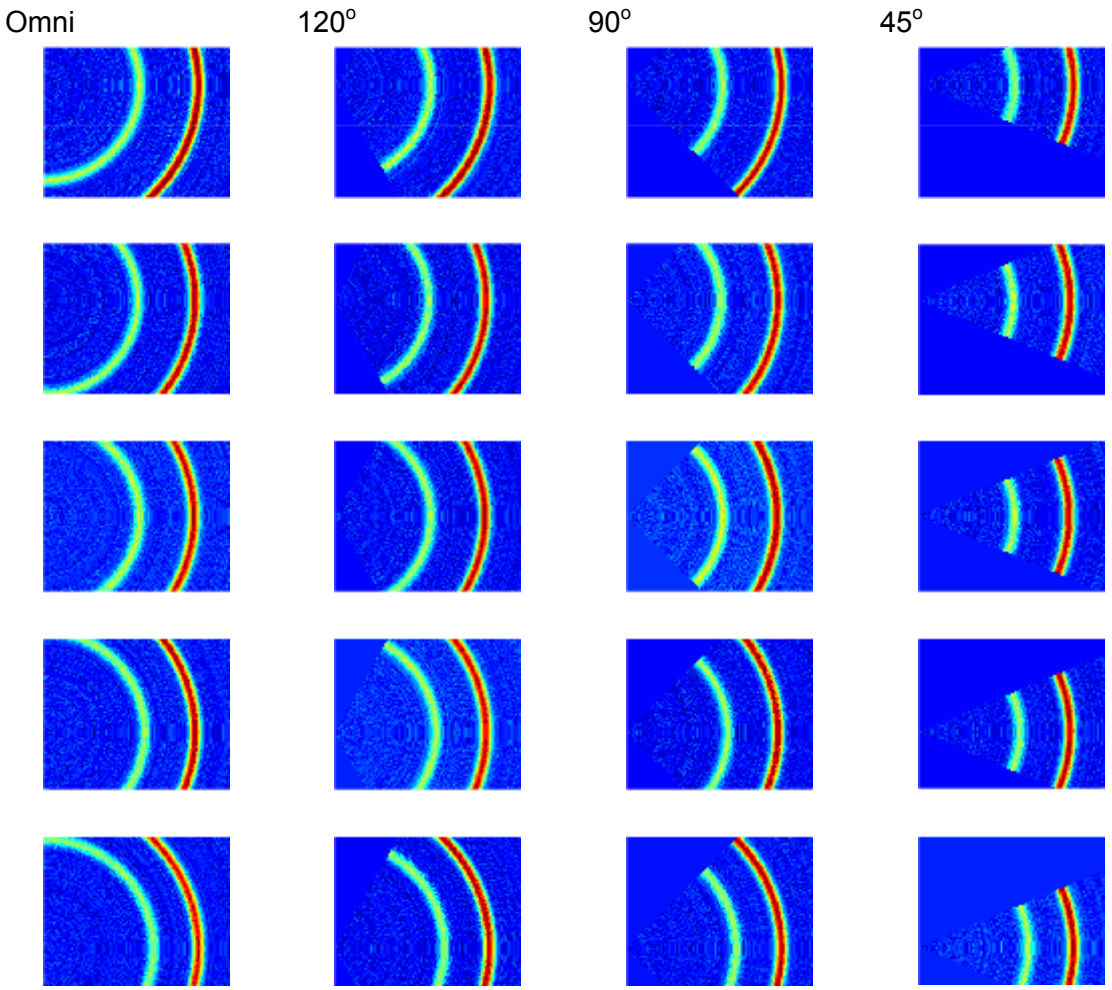

Figure 13. *Image maps corresponding to discrete radar platform positions.*

As successive images corresponding to individual element positions are added, the grid points where arcs overlap tend to be reinforced while other regions fade (Figure 14). A major component of image processing therefore, is constructive interference.

Omni

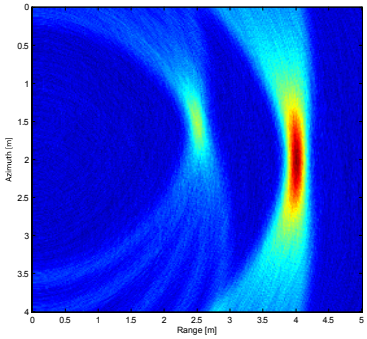

120°

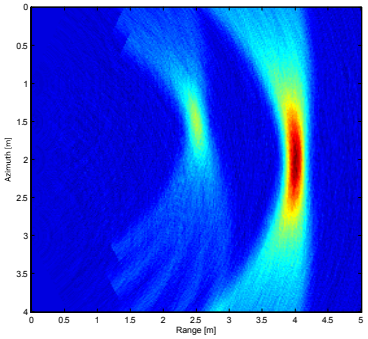

90°

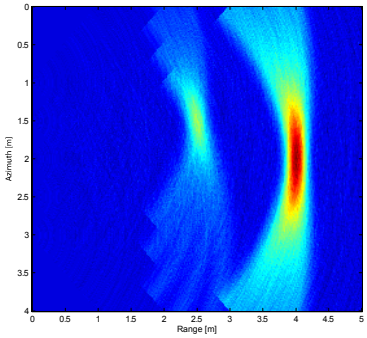

45°

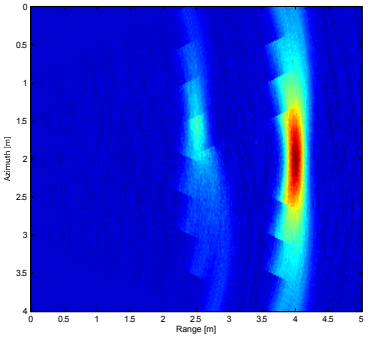

Figure 14. *Reconstructed images corresponding to Figure 13.*

In the table below, loop efficiency reflects the reduction in the number of iterations required to work through the imaging grid as in Figure 14. The image quality criterion is the full-width at half-maximum (FWHM).

Table 1. *Comparison of processing efficiency*
(Target at range 2.5m, Synthetic aperture 2.0m)

Beamwidth	Loop efficiency [%]	FWHM [m]
omni	0.0	1.07
120°	12.8	1.01
90°	22.3	1.12
45°	51.6	1.25

3.3 Restricted beamwidth processing for 3D

Having established this method for the 2D case, we can now (with suitable generalizations) apply it to three-dimensional imaging. The main principle remains the

same: take one step downrange and adjust the grid point indices to account for the antenna beam pattern. For the 3D case, instead of determining segment length along the azimuth, L_x^j, we now consider two segments in the x-z plane, namely L_x^j and L_z^j. Once again, *j* is the index for the range coordinate.

To account for the volume illuminated by the antenna, we specify two angles where Θ is the horizontal beamwidth and Φ is the vertical beamwidth. This leads to the half-beamwidth angles $\alpha = \Theta/2$ and $\beta = \Phi/2$. In turn, this results in —

$$L_x^j = (\delta r + j\Delta y)\tan\alpha \qquad (9)$$

$$L_z^j = (\delta r + j\Delta y)\tan\beta \qquad (10)$$

These quantities are shown in Figure 15 as projections on the *xz* plane at a given range. In general the shaded area will be elliptical, but to simplify calculations the projection is assumed to be rectangular.

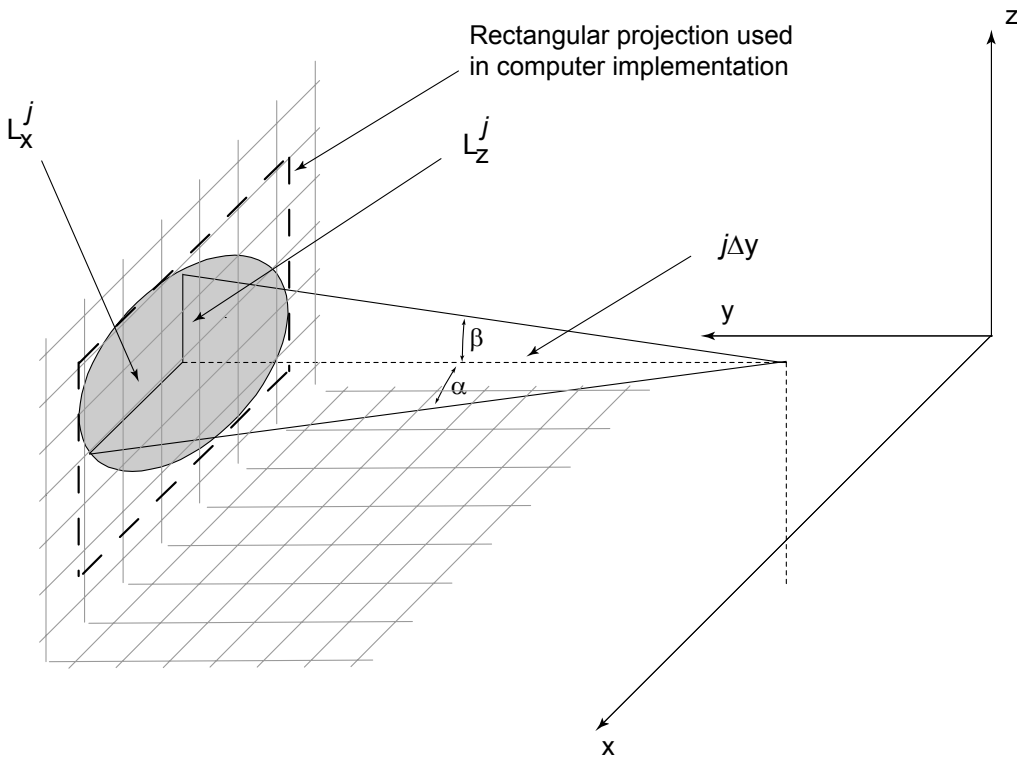

Figure 15. *Projection of beam in 3D coordinate system.*

Following the same reasoning as before, the indices for *x*- and *z*- grid points are restricted to:

$$\left\lceil \frac{x^n - L_x^j}{\Delta x} \right\rceil \;:\; i \;:\; \left\lfloor \frac{x^n + L_x^j}{\Delta x} \right\rfloor \qquad (11)$$

and

$$\left\lfloor \frac{z^m + L_z^j}{\Delta z} \right\rfloor \;:\; k \;:\; \left\lceil \frac{z^m - L_z^j}{\Delta z} \right\rceil \qquad (12)$$

To consider a more accurate depiction of how the antenna beam projects onto the *xz* plane, one could consider an ellipse (Figure 16), as it would account for both horizontal and vertical beamwidths.

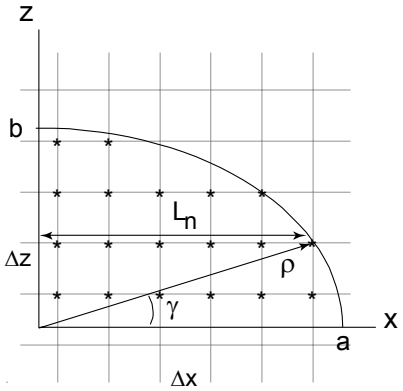

Figure 16. *Interpolation of grid points for elliptic projection.*

However, it would be necessary to calculate grid points as an *implicit* function of ρ, γ, and Δz. The problem stems from the fact that ρ will change depending on the value of $z = n\Delta z$. To make matters worse, you need to know the extent of the major and minor axes to obtain

$$\rho = \frac{b^2}{1 - e^2 \cos^2 \gamma} \qquad (13)$$

where $e^2 = 1 - b^2 / a^2$.

To determine the horizontal extent of the ellipse, and consequently the min/max loop indices, we would have to determine

$$L_n = \sqrt{\left(\frac{b^2}{1 - e^2 \cos^2 \gamma} \right)^2 - (n\Delta z)^2} \qquad (14)$$

for each elevation increment. This would cause excessive cpu time and it is suggested that the *xz* projection remain rectangular.

4. Conclusion

In this report, two-dimensional synthetic aperture radar (SAR) is generalized for three-dimensional imaging application, for both data and image processing operations. The key to effective algorithm implementation is having a clear, consistent description of the required processing steps—these have been illustrated graphically and with the governing equations.

Rather than frequency-domain based reconstruction, the time-domain method of backprojection was selected for this application. This is simple to implement, generates localized sidelobes, and it can handle path adjustments for motion compensation and propagation through a dielectric layer such as a building wall.

Another advantage of backprojection is that intermediate stages of computation are intuitive and easily visualized since there are no time-frequency transformations. For example, resolution in elevation is limited by the physical length of the linear array, but another view of how these limitations arise was presented based on the focusing of returns in 3D data space, $d(x, z, t)$.

As this is currently envisioned as a ground-based application, positioning errors arising from the arbitrary orientation of a linear array moving across irregular terrain need to be considered. A full analysis was not undertaken, but the basic problem was outlined, along with a description of how the situation could be simulated. This will take on greater significance when motion compensation is considered in the future.

A major drawback with backprojection is the severe computational requirement of having to loop over every grid point in image space. A method to restrict the area or volume by adjusting loop indices was described. This results in a smaller area of illumination within the target area, producing a more realistic scenario. Initial results show that depending on the width of the effective beam, the number of loops can be reduced by up to 50%, while still maintaining good image quality in terms of the reconstructed target response FWHM. Potential improvements in 3D SAR processing are even greater.

Simulations indicate there will be an optimum value for the beamwidth. The omnidirectional beam commonly used provides good results at the cost of excessive iterations. A narrow beamwidth is more efficient, but the image quality is impaired–a major aspect of SAR processing is building up an image by viewing it from many positions. This angular diversity is enhanced by using a broad-beam antenna, so the simulations support the intuition that the best setting will be somewhere between the two extremes, and that incorporating the antenna pattern into the backprojection method will result in more effective and efficient image reconstruction.

5. References

1. Soumekh, M. (1999). Synthetic Aperture Radar Signal Processing with MATLAB Algorithms. New York: John Wiley and Sons, Inc..

2. Barrie, G. (2003). Ultra-wideband Synthetic Aperture Imaging – Data and Image Processing, (DRDC Ottawa TM 2003-015), Defence R&D Canada – Ottawa.

3. Boutros, J. & Barrie, G. (2003). Ultra-wideband Synthetic Aperture Radar Imaging: Effect of off-track motion on resolution, (DRDC Ottawa TM 2003-177), Defence R&D Canada – Ottawa.

This page intentionally left blank.

DOCUMENT CONTROL DATA

(Security classification of title, body of abstract and indexing annotation must be entered when the overall document is classified)

1. ORIGINATOR (the name and address of the organization preparing the document. Organizations for whom the document was prepared, e.g. Establishment sponsoring a contractor's report, or tasking agency, are entered in section 8.)

   Defence R&D Canada – Ottawa
   Ottawa, Ontario K1A 0Z4

2. SECURITY CLASSIFICATION (overall security classification of the document, including special warning terms if applicable)

   UNCLASSIFIED

3. TITLE (the complete document title as indicated on the title page. Its classification should be indicated by the appropriate abbreviation (S,C or U) in parentheses after the title.)

   Through-Wall Synthetic Aperture Radar (TWSAR) 3D Imaging: Algorithm Design (U)

4. AUTHORS (Last name, first name, middle initial)

   Barrie, Greg, B.

5. DATE OF PUBLICATION (month and year of publication of document)	6a. NO. OF PAGES (total containing information. Include Annexes, Appendices, etc.)	6b. NO. OF REFS (total cited in document)
November 2004	32	3

7. DESCRIPTIVE NOTES (the category of the document, e.g. technical report, technical note or memorandum. If appropriate, enter the type of report, e.g. interim, progress, summary, annual or final. Give the inclusive dates when a specific reporting period is covered.)

   Technical Memorandum

8. SPONSORING ACTIVITY (the name of the department project office or laboratory sponsoring the research and development. Include the address.)

9a. PROJECT OR GRANT NO. (if appropriate, the applicable research and development project or grant number under which the document was written. Please specify whether project or grant)	9b. CONTRACT NO. (if appropriate, the applicable number under which the document was written)
Project # 12KC15	

10a. ORIGINATOR'S DOCUMENT NUMBER (the official document number by which the document is identified by the originating activity. This number must be unique to this document.)	10b. OTHER DOCUMENT NOS. (Any other numbers which may be assigned this document either by the originator or by the sponsor)
DRDC Ottawa TM 2004-224	

11. DOCUMENT AVAILABILITY (any limitations on further dissemination of the document, other than those imposed by security classification)

- (x) Unlimited distribution
- ( ) Distribution limited to defence departments and defence contractors; further distribution only as approved
- ( ) Distribution limited to defence departments and Canadian defence contractors; further distribution only as approved
- ( ) Distribution limited to government departments and agencies; further distribution only as approved
- ( ) Distribution limited to defence departments; further distribution only as approved
- ( ) Other (please specify):

12. DOCUMENT ANNOUNCEMENT (any limitation to the bibliographic announcement of this document. This will normally correspond to the Document Availability (11). However, where further distribution (beyond the audience specified in 11) is possible, a wider announcement audience may be selected.)

13. ABSTRACT (a brief and factual summary of the document. It may also appear elsewhere in the body of the document itself. It is highly desirable that the abstract of classified documents be unclassified. Each paragraph of the abstract shall begin with an indication of the security classification of the information in the paragraph (unless the document itself is unclassified) represented as (S), (C), or (U). It is not necessary to include here abstracts in both official languages unless the text is bilingual).

Typical synthetic aperture radar (SAR) images are two-dimensional, providing range and azimuth information, but furnish few details with respect to elevation. One approach to extend SAR to three-dimensional imaging is to replace the single antenna element by an array of antenna elements. The simplest such implementation of this would be a linear array oriented vertically. This report contains two sections, the first outlining data and image processing for a three-dimensional application, and the second part details finite beamwidth processing for the time-domain backprojection method. Standard backprojection implicitly assumes infinite beamwidth, whereby the entire target area is illuminated and returns are collected from all points in the imaging grid. This decreases the efficiency of the algorithm by summing over unnecessary grid points. Finite beamwidth processing is designed to be more physically realistic by accounting for the actual antenna pattern. Initial results show that depending on the width of the effective beam, the number of processing loops can be reduced by up to 50%, while still maintaining good image quality in terms of the reconstructed target response (pulse width). Potential improvements in 3D SAR processing are even greater.

14. KEYWORDS, DESCRIPTORS or IDENTIFIERS (technically meaningful terms or short phrases that characterize a document and could be helpful in cataloguing the document. They should be selected so that no security classification is required. Identifiers such as equipment model designation, trade name, military project code name, geographic location may also be included. If possible keywords should be selected from a published thesaurus. e.g. Thesaurus of Engineering and Scientific Terms (TEST) and that thesaurus-identified. If it is not possible to select indexing terms which are Unclassified, the classification of each should be indicated as with the title.)

Through-Wall, Through-Wall Sensing, three-dimensional imaging, SAR, backprojection, reduced beamwidth

Defence R&D Canada

Canada's leader in defence
and national security R&D

R & D pour la défense Canada

Chef de file au Canada en R & D
pour la défense et la sécurité nationale

www.drdc-rddc.gc.ca